Chemical Physics 85 (1984) 149–164
North-Holland, Amsterdam

HOPPING TRANSPORT ON A RANDOMLY SUBSTITUTED LATTICE IN THE PRESENCE OF DILUTE DEEP TRAPS

Roger F. LORING, Hans C. ANDERSEN and M.D. FAYER
Department of Chemistry, Stanford University, Stanford, California 94305, USA

Received 31 August 1983

Our recent theory of hopping transport of excitations or charge carriers among particles randomly distributed on the sites of a lattice is extended here to include the presence of a low concentration trap species. We present an exact diagrammatic analysis of the configuration-averaged Green function of the Pauli master equation for this problem. We obtain a non-perturbative approximation to the Green function that is expected to be accurate at both high and low donor concentration for low trap concentration. The approximation can be carried out for any lattice type in which any two sites can be transformed into one another by a symmetry operation, and a transfer rate of any distance dependence. We present calculations of the observable in a steady-state excitation transfer and trapping experiment that illustrate the effect of dimensionality and of the distance dependence of the transfer rate on this observable.

1. Introduction

In a recent paper [1], hereafter referred to as I, we presented a theory of hopping transport of electrons or optical excitations among particles randomly distributed on the sites of a lattice. The results in I can be used to calculate transport properties for a transfer rate of any distance dependence on any lattice in which any two sites can be transformed into one another by a symmetry operation. The theory provides excellent approximations for both high and low concentrations. In the present work we extend the treatment of I to include a deep trap species that is present in low concentration. This modification makes the previous theory applicable to a larger group of experiments. Transport in the presence of traps is intrinsically interesting, and must be understood for the practical reason that low concentration traps are necessarily present in crystals of all types. For example, chemical [2–5] and defect [6] traps have been studied in molecular crystals, and chromium dimer traps have been studied in ruby [7].

The theoretical problem of incoherent transport among randomly distributed particles in the presence of traps has been addressed by several investigators. Most workers have used a continuum model in which donor and trap points are randomly distributed in a volume [8–13]. As discussed in section 4, it can be inappropriate to apply a continuum model to experimental data on crystals. Sakun [14] has developed a theory of transport and trapping on a randomly substituted lattice, but unlike the results presented here, his work is only valid for low donor concentration. Kenkre and Parris [15] have presented a theory of trapping by interstitial traps randomly placed in a fully occupied lattice of donors. Since their method takes advantage of the translational invariance of the donor array, it does not appear to be extendable to the situation treated here, in which the donors and traps are randomly distributed on the sites of a partially filled lattice.

Section 2 contains a summary of an exact analysis of the configuration-averaged Pauli master equation Green function for the trapping problem. The exact diagrammatic expansion of the Green function is given in appendix A. Section 3 contains a description of our lattice two-body approximation for dilute traps, which should be valid over the full range of donor concentration. Some of the details of the calculation are

0301-0104/84/$03.00

given in appendices B and C. In section 4, we present calculations of the observable in steady-state excitation transfer and trapping experiments and discuss the effect of the dimensionality and of the distance dependence of the transfer rate on this observable. We also show that the results of such experiments on isotopically mixed naphthalene crystals [5] can be described by our model with an octupole–octupole transfer rate. The theory presented here is expected to provide an accurate description of hopping transport of excited states or charge carriers in the presence of dilute deep traps for any lattice type, any transfer rate and any donor concentration.

2. The configuration-averaged Green function

The system consists of N_D donors labeled 1 through N_D and N_T deep traps labeled N_D+1 through N_D+N_T distributed randomly among the M sites of a lattice. All configurations of the donors and traps are assumed to be equally likely, so a given site has a probability $c_D = N_D/M$ of being occupied by a donor and a probability $c_T = N_T/M$ of being occupied by a trap. In the following discussion we will refer to the entity being transferred as an excitation, but the methods and results apply equally well to the charge carrier transfer problem. $P_j(\boldsymbol{R}, t)$, the probability that the jth particle is excited at time t in a particular configuration $\boldsymbol{R} = (\boldsymbol{r}_1, \boldsymbol{r}_2 \cdots \boldsymbol{r}_{N_D+N_T})$ is taken to satisfy the Pauli master equation

$$\mathrm{d}\boldsymbol{P}(\boldsymbol{R}, t)/\mathrm{d}t = \mathbf{Q}\cdot\boldsymbol{P}(\boldsymbol{R}, t), \tag{1}$$

where $P_j(\boldsymbol{R}, t)$ is the jth element of the (N_D+N_T)-dimensional vector $\boldsymbol{P}(\boldsymbol{R}, t)$. $\mathbf{Q}$ is an (N_D+N_T)-dimensional square matrix given by

$$\begin{aligned}
&Q_{jk} = w_{jk} - \delta_{jk}\left(\sum_{l=1}^{N_D} w_{lk} + \sum_{i=N_D+1}^{N_D+N_T} v_{ik}\right), && j, k \leqslant N_D;\\
&Q_{jk} = v_{jk}, && N_D < j \leqslant N_D+N_T, \quad k \leqslant N_D;\\
&Q_{jk} = 0, && k > N_D.
\end{aligned} \tag{2}$$

In this model, an excitation may be transferred from a donor to a donor or from a donor to a trap, but transfer from a trap either to another trap or to a donor is forbidden. $w_{kj} = w_{jk}$ is the transfer rate between donors j and k and v_{nl} is the transfer rate between donor l and trap n. w_{jj} is defined to be zero. δ_{jk} is the Kronecker delta. w_{jk} and v_{nl} are assumed to depend only on the vector distance between the two particles. We assume initially that the lifetimes of the excitation on the donor and the trap are infinite, as is the case if the "excitation" is a charge carrier. Transport properties for the case in which the excitation has finite lifetimes on donor and trap may be easily obtained from transport properties for the infinite lifetimes case, as shown in refs. [12,13]. This matter will be discussed further in section 4.

We wish to calculate the configuration-averaged Green function, from which the system's transport properties can be obtained. The Green function $G(\boldsymbol{r}, \boldsymbol{r}', t)$ gives the probability that an excitation has migrated from position $\boldsymbol{r}'$ to position $\boldsymbol{r}$ in time t. $G(\boldsymbol{r}, \boldsymbol{r}', t)$ can be written as the sum of three terms:

$$G(\boldsymbol{r}, \boldsymbol{r}', t) = \delta_{\boldsymbol{r},\boldsymbol{r}'}G^{\mathrm{s}}(t) + G^{\mathrm{m}}(\boldsymbol{r}-\boldsymbol{r}', t) + G^{\mathrm{T}}(\boldsymbol{r}-\boldsymbol{r}', t), \tag{3}$$

$$G^{\mathrm{s}}(t) = \langle(\mathrm{e}^{t\mathbf{Q}})_{11}\rangle, \qquad G^{\mathrm{m}}(\boldsymbol{r}-\boldsymbol{r}', t) = (N_D-1)\langle(\mathrm{e}^{t\mathbf{Q}})_{21}\delta_{\boldsymbol{r}_{21},\boldsymbol{r}-\boldsymbol{r}'}\rangle,$$

$$G^{\mathrm{T}}(\boldsymbol{r}-\boldsymbol{r}', t) = N_T\langle(\mathrm{e}^{t\mathbf{Q}})_{N_D+1,1}\delta_{\boldsymbol{r}_{(N_D+1)1},\boldsymbol{r}-\boldsymbol{r}'}\rangle \tag{4}$$

$G^{\mathrm{s}}(t)$ is the probability that a donor excited at $t=0$ retains its excitation after a time t. $G^{\mathrm{m}}(\boldsymbol{r}-\boldsymbol{r}', t)$ is the probability that an excitation has migrated from a donor at position $\boldsymbol{r}'$ to a donor at a distinct position

r in time t. $G^{T}(r-r', t)$ is the probability that an excitation has migrated from a donor at position r' to a trap at position r in time t. The angular brackets in eqs. (4) denote a lattice configuration average [1] defined by

$$\langle F(R)\rangle = \left(\sum_{r_1,\cdots r_{N_D+N_T}} F(R)\prod_{i<j}\left(1-\delta_{r_i,r_j}\right)\right)\left(\sum_{r_1,\cdots r_{N_D+N_T}}\prod_{i<j}\left(1-\delta_{r_i,r_j}\right)\right)^{-1} \tag{5}$$

The sums over donor and trap positions r_j run over all sites in the lattice.

We now follow the analysis of the Green function originally presented for the continuum transport problem by Gochanour et al. [16], which is adapted in refs. [12,13] to the continuum transport and trapping problem and in I to the lattice transport problem. The Fourier–Laplace transform of the Green function is given by

$$\hat{G}(k,\epsilon) = \int_0^\infty dt\, e^{-\epsilon t}\sum_r e^{ik\cdot r} G(r,t). \tag{6}$$

We expand $\hat{G}(k,\epsilon)$ in a perturbation series in powers of $\mathbf{Q}$. The Fourier–Laplace transforms of eqs. (4) are written as infinite series of lattice sums over products of w_{ij} and v_{ij} transfer rates. Each such lattice sum is represented by a diagram. Diagrammatic expansions in the thermodynamic limit [1] of $\hat{G}^{m}(k,\epsilon)$, $\hat{G}^{T}(k,\epsilon)$ and $\hat{G}^{s}(\epsilon)$ are given in appendix A. $\hat{G}^{m}(k,\epsilon)$ can be written in terms of a quantity $\Sigma_D(k,\hat{G}^{s}(\epsilon))^{\star}$, which is equal to the sum of a subset of $\hat{G}^{m}(k,\epsilon)$ diagrams. Similarly, $\hat{G}^{T}(k,\epsilon)$ can be expressed in terms of $\Sigma_T(k,\hat{G}^{s}(\epsilon))$, which is equal to the sum of a subset of $\hat{G}^{T}(k,\epsilon)$ diagrams *. Both $\Sigma_D(k,\hat{G}^{s}(\epsilon))$ and $\Sigma_T(k,\hat{G}^{s}(\epsilon))$ are functionals of $\hat{G}^{s}(\epsilon)$. Their diagrammatic expansions are given in appendix A. $\hat{G}^{m}$ and $\hat{G}^{T}$ are related to Σ_D and Σ_T by

$$\hat{G}^{m}(k,\epsilon) = \frac{c_D\left[\hat{G}^{s}(\epsilon)\right]^2\Sigma_D\left(k,\hat{G}^{s}(\epsilon)\right)}{1-c_D\hat{G}^{s}(\epsilon)\Sigma_D\left(k,\hat{G}^{s}(\epsilon)\right)}, \qquad \hat{G}^{T}(k,\epsilon) = \frac{c_T\left[\hat{G}^{s}(\epsilon)/\epsilon\right]\Sigma_T\left(k,\hat{G}^{s}(\epsilon)\right)}{1-c_D\hat{G}^{s}(\epsilon)\Sigma_D\left(k,\hat{G}^{s}(\epsilon)\right)}. \tag{7}$$

From the Fourier–Laplace transform of eq. (3), the fact that $\lim_{k\to 0}\hat{G}(k,\epsilon) = 1/\epsilon$ (conservation of probability), and eqs. (7), we can derive an exact relation between $\hat{G}^{s}(\epsilon)$ and the $k\to 0$ limits of $\Sigma_D(k,\hat{G}^{s})$ and $\Sigma_T(k,\hat{G}^{s})$.

$$\hat{G}^{s}(\epsilon) = \frac{1}{\epsilon + c_D\Sigma_D\left(0,\hat{G}^{s}(\epsilon)\right) + c_T\Sigma_T\left(0,\hat{G}^{s}(\epsilon)\right)} \tag{8}$$

An exact expression for the Laplace transform of the probability that an excitation remains somewhere in the donor ensemble after a time t can also be derived in terms of Σ_T and Σ_D. We define $G^{D}(r,t)$ as the sum of $G^{s}(r,t)$ and $G^{m}(r,t)$. $G^{D}(r,t)$ gives the probability that an excitation has undergone a displacement r within the donor ensemble in time t. The Fourier–Laplace transform of this quantity is given by

$$\hat{G}^{D}(k,\epsilon) = \frac{\hat{G}^{s}(\epsilon)}{1-c_D\hat{G}^{s}(\epsilon)\Sigma_D\left(k,\hat{G}^{s}(\epsilon)\right)}. \tag{9}$$

The $k\to 0$ limit of eq. (9) gives the Laplace transform of the probability that an excitation has not been trapped during a time t.

All of the results presented thus far are exact. If Σ_D and Σ_T could be evaluated exactly, then $\hat{G}^{s}(\epsilon)$ could be obtained exactly from eq. (8). Substitution of the exact $\hat{G}^{s}(\epsilon)$, Σ_D, and Σ_T into eqs. (7) would yield $\hat{G}^{m}(k,\epsilon)$ and $\hat{G}^{T}(k,\epsilon)$ and hence the entire Green function.

* $[\hat{G}^{s}(\epsilon)]^2\, c_D\, \Sigma_D(k,\hat{G}^{s}(\epsilon))$ and $[\hat{G}^{s}(\epsilon)/\epsilon]\, c_T\Sigma_T(k,\hat{G}^{s}(\epsilon))$ correspond to the quantities $\Delta(k,\hat{G}^{s}(\epsilon))$ and $\Gamma(k,\epsilon,\hat{G}^{s}(\epsilon))$ defined for the continuum transport and trapping problem in refs. [12,13].

3. Two-body approximation to Σ_D and Σ_T for $c_T \ll 1$

Since the diagrammatic series for Σ_D and Σ_T (eqs. (A6) and (A7)) cannot be summed exactly, we resort to the approximation procedure of refs. [1,12,16]. We carry out a partial summation of the Σ_D and Σ_T series to obtain approximations of these quantities as functionals of $\hat{G}^s(\epsilon)$. When these approximations are substituted into eq. (8) the result is an equation with $\hat{G}^s$ as the only unknown. This equation can be solved for a non-perturbative approximation to $\hat{G}^s$ as a function of the Laplace variable ϵ and the donor and trap concentrations c_D and c_T. The rest of the Green function can then be approximated from eqs. (7).

In I, a hierarchy of approximations was proposed to the Σ_D series for the lattice transport problem in the absence of traps:

$$\Sigma_D(k, \hat{G}^s(\epsilon)) \approx \sum_{i=2}^{n} \Sigma_D^{(i)}(k, \hat{G}^s(\epsilon)), \tag{10}$$

where $\Sigma_D^{(i)}$ is the sum of all diagrams that can be evaluated by performing a lattice sum over i independent particle positions. The approximation in eq. (10) is denoted the n-body approximation. As discussed in I, the lattice n-body approximation to Σ_D is not simply an expansion in powers of c_D. It contains terms of all order in c_D as well as all diagrams of order c_D^{n-1} or lower. It was shown in I that the two-body approximation to Σ_D as defined in eq. (10) with $n = 2$ gives transport properties that are accurate in the $c_D \to 0$ limit and gives the exact generalized diffusion coefficient at $c_D = 1$. We therefore expect that two-body approximations to Σ_D and Σ_T for the transport and trapping problem will also be accurate for both high and low donor and trap concentrations.

The evaluation of the two-body approximations to Σ_D and Σ_T in the transport and trapping problem is considerably more complicated than the evaluation of the two-body Σ_D carried out in I. In this work we will restrict ourselves to the experimentally important situation in which the donors may be present in any concentration, but the trap concentration is much smaller than unity. We approximate Σ_D and Σ_T by $\bar{\Sigma}_D^{(2)}$ and $\bar{\Sigma}_T^{(2)}$, the subset of $\Sigma_D^{(2)}$ and $\Sigma_T^{(2)}$ diagrams that are of order c_T^0 or c_T. If $c_T \ll 1$, it is valid to neglect terms of order c_T^2 and higher, and the resulting approximations to Σ_D and Σ_T should yield transport properties that are accurate for any value of c_D.

The contribution to $\Sigma_D^{(2)}$ that is of order c_T^0 was evaluated in I. The evaluation of the remaining terms that compose $\bar{\Sigma}_D^{(2)}$ and $\bar{\Sigma}_T^{(2)}$ is discussed in appendices B and C. The resulting formulae for $\bar{\Sigma}_D^{(2)}$ and $\bar{\Sigma}_T^{(2)}$ are as follows:

$$\begin{aligned}
\bar{\Sigma}_D^{(2)}(k, \hat{G}^s(\epsilon)) = {} & \sum_r w(r) \int_0^\infty d\alpha\, e^{-\alpha} \frac{e^{-z\alpha}}{1 - c_D + c_D e^{-z\alpha}} \\
& \times \left((1/c_D) \ln(1 - c_D + c_D e^{-z\alpha}) + \frac{e^{-z\alpha}}{1 - c_D + c_D e^{-z\alpha}} (e^{ik\cdot r} - 1) + 1 \right) \\
& - 2c_T \sum_r e^{ik\cdot r} w(r) \left[\int_0^\infty d\alpha\, e^{-\alpha} \frac{e^{-z\alpha}}{1 - c_D + c_D e^{-z\alpha}} \right. \\
& \left. \times \left(\frac{\theta e^{-z\alpha\theta}}{(1 - c_D + c_D e^{-z\alpha\theta})^2} - \frac{e^{-z\alpha}}{(1 - c_D + c_D e^{-z\alpha})^2} \right) \right] \\
& - c_T \sum_r w(r) \int_0^\infty d\alpha\, e^{-\alpha} \left((1/c_D) \ln(1 - c_D + c_D e^{-z\alpha}) + \frac{(1 - c_D)(1 - e^{-z\alpha})}{1 - c_D + c_D e^{-z\alpha}} \right)
\end{aligned}$$

$$\times\left(\frac{\theta^2 e^{-z\alpha\theta}}{(1-c_D+c_D e^{-z\alpha\theta})^2}-\frac{e^{-z\alpha}}{(1-c_D+c_D e^{-z\alpha})^2}\right)$$

$$-2c_T\sum_r w(r)\int_0^\infty d\alpha\, e^{-\alpha}\frac{e^{-z\alpha}}{1-c_D+c_D e^{-z\alpha}}$$

$$\times\left(\frac{e^{-z\alpha}+(1-c_D)/2c_D}{(1-c_D+c_D e^{-z\alpha})^2}-\frac{e^{-z\alpha\theta}+(1-c_D)/2c_D}{(1-c_D+c_D e^{-z\alpha\theta})^2}\right), \tag{11}$$

$$\bar{\Sigma}_T^{(2)}(k,\hat{G}^s(\epsilon))=-c_D\sum_r zv(r)(1-\theta e^{ik\cdot r})\int_0^\infty d\alpha\, e^{-\alpha}\frac{e^{-z\alpha}}{1-c_D+c_D e^{-z\alpha}}$$

$$\times\frac{\theta e^{-z\alpha\theta}}{(1-c_D+c_D e^{-z\alpha\theta})^2}+\sum_r e^{ik\cdot r}v(r)\theta. \tag{12}$$

In the above equations, $z\equiv\hat{G}^s(\epsilon)w(r)$ and $\theta\equiv 1/[1+\hat{G}^s(\epsilon)v(r)]$.

4. Application to steady-state energy transport and trapping experiments

Transport and trapping of excited states have been studied in a variety of mixed molecular crystals using steady-state optical experiments [2–5]. It is generally found that for low trap concentration the fraction of luminescence from the traps is strongly dependent on donor concentration. For low donor concentrations, the relative trap luminescence increases slowly with increasing donor concentration until a critical concentration is reached at which trapping becomes very efficient and a substantial fraction of the total luminescence comes from the traps. This effect is easy to interpret qualitatively for a system in which the trap concentration is low and interactions are of short range, so that most trapping events are preceded by a series of donor–donor hops. At low donor concentrations, most excitations will be restricted to small clusters of donors and little trapping will occur. As the donor concentration is raised, a concentration will be reached at which the donor system is sufficiently connected that paths of interacting donors will lead to most traps, and most of the excitations will be trapped. Thus, measurements of the relative trap luminescence at fixed low trap concentration as a function of donor concentration will yield information about the extent of donor to donor transport in the system.

It is shown in ref. [13] that the fraction of trap luminescence in an energy transfer experiment in which the excitation has finite lifetimes on donor and trap can be calculated in a straightforward way from the Green function for the transport problem in which the excitation is taken to have

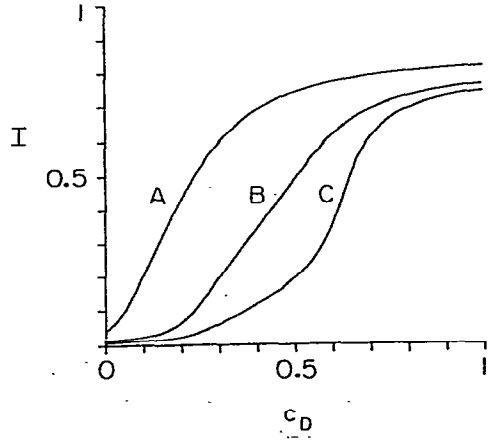

Fig. 1. $I(c_D, c_T)$ from eq. (13) for a square lattice with $q_D/q_T=1$ and $c_T=10^{-3}$. (A) $w(r)=v(r)=k_D(R/r)^6$; $a/R=0.304$. (B) $w(r)=v(r)=k_D(R/r)^{10}$; $a/R=0.489$. (C) $w(r)=v(r)=k_D(R/r)^{14}$; $a/R=0.600$. The ratio of lattice spacing a to interaction length R has been chosen so that $w(a)$ is the same for the three cases. These three curves illustrate the influence of long-range transfer steps on $I(c_D, c_T)$.

infinite lifetimes on donor and trap:

$$I(c_D,c_T)=\frac{1-k_D\hat{G}^D(0,k_D)}{1+k_D\hat{G}^D(0,k_D)(q_D/q_T-1)}. \quad (13)$$

$I(c_D, c_T)$ is the integrated trap luminescence normalized by the sum of the integrated luminescence from donors and traps. k_D is the inverse of the donor lifetime. q_D and q_T are the donor and trap quantum yields (ratio of measured lifetime to radiative lifetime) in the absence of energy transfer. $\hat{G}^D(k, \epsilon)$ is defined in eq. (9). The experimental observable $I(c_D, c_T)$ can be calculated for small c_T within the two-body approximation from eqs. (11), (12), (8) and (9). Since $I(c_D, c_T)$ is a steady-state observable, it can be calculated directly from the Laplace transform of the Green function.

The two-body results presented here allow the calculation of the Green function for arbitrary lattice type (provided that any two sites can be transformed into one another by a symmetry operation) and for transfer rates of arbitrary distance dependence. In fig. 1, we illustrate the importance of long-range interactions in determining the observable $I(c_D, c_T)$. These calculations were carried out for a square lattice, a trap mole fraction of 10^{-3} and equal donor and trap quantum yields. In curve A, the donor–donor and donor–trap transfer rates are taken to be $w(r)=v(r)=k_D(R/r)^6$ (orientation-averaged dipole–dipole rate). In curve B, the rates are $w(r)=v(r)=k_D(R/r)^{10}$ (orientation-averaged quadrupole–quadrupole rate). In curve C, the rates are $w(r)=v(r)=k_D(R/r)^{14}$ (orientation-averaged octupole–octupole rate). In each case the ratio of the lattice spacing a to the interaction length R has been chosen so that the step rate evaluated at the nearest-neighbor distance is the same in all three cases (≈ 1300 hops/lifetime). Thus the three plots differ only in the extent to which there are interactions outside the first shell of neighbors. Although each of the transfer rates is a sharply decreasing function of distance, this difference is sufficient to dramatically change the dependence of $I(c_D, c_T)$ on c_D for fixed small c_T. In the limit of a transfer rate that is non-zero only to nearest neighbors, the observable $I(c_D, c_T)$ for small c_D should be near zero below the critical concentration for site percolation, and then rise steeply at that concentration, which for the square lattice is 0.59 [17]. It can be easily shown that for a nearest-neighbor transfer rate on a square lattice there is a range of donor concentrations around the critical concentration for which there exist no physically reasonable solutions of eq. (8) in the two-body approximation, i.e. solutions that are real continuous functions of ϵ for $\epsilon \geq 0$. For the corresponding problem on a cubic lattice, physically reasonable solutions exist for all donor concentrations.

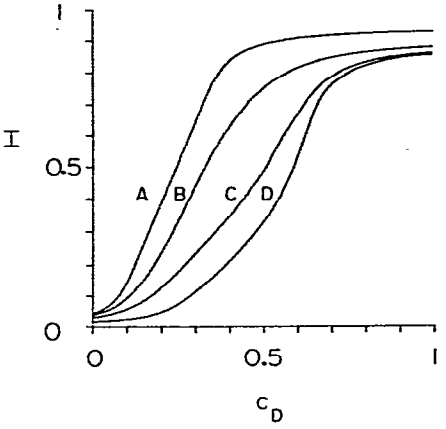

Fig. 2. $I(c_D, c_T)$ from eq. (13) for $c_T=10^{-3}$, $q_D/q_T=0.5$, $a/R=0.60$ and $w(r)=v(r)=k_D(R/r)^{14}$. (A) Simple cubic lattice of spacing a. (B) Orthorhombic lattice with spacing a in the xy plane and spacing a_z in the z direction. $w(a_z)=0.1\ w(a)$. (C) Orthorhombic lattice with spacing a in the xy plane and spacing a_z in the z direction. $w(a_z)=0.01\ w(a)$. (D) Square lattice of spacing a. This figure illustrates the influence of dimensionality on this observable.

Fig. 2 illustrates the influence of dimensionality on the trapping observable. Curve A shows $I(c_D, c_T)$ for $c_T=10^{-3}$, $q_D/q_T=0.5$, $w(r)=v(r)=k_D(R/r)^{14}$ and $a/R=0.60$, for a simple cubic lattice and curve D shows $I(c_D, c_T)$ for the same parameters with a square lattice. The other two plots show $I(c_D, c_T)$ for orthorhombic lattices in which the transfer rate evaluated at the nearest-neighbor distance in the z direction is 1% of that rate in the xy plane (curve C) and 10% of that rate (curve B). Most molecular crystal energy transport systems are very anisotropic and are often modeled with isotropic lattices of lower dimensionality [4,5]. Fig. 2 shows that adding a small amount of transfer in a third dimension changes $I(c_D, c_T)$

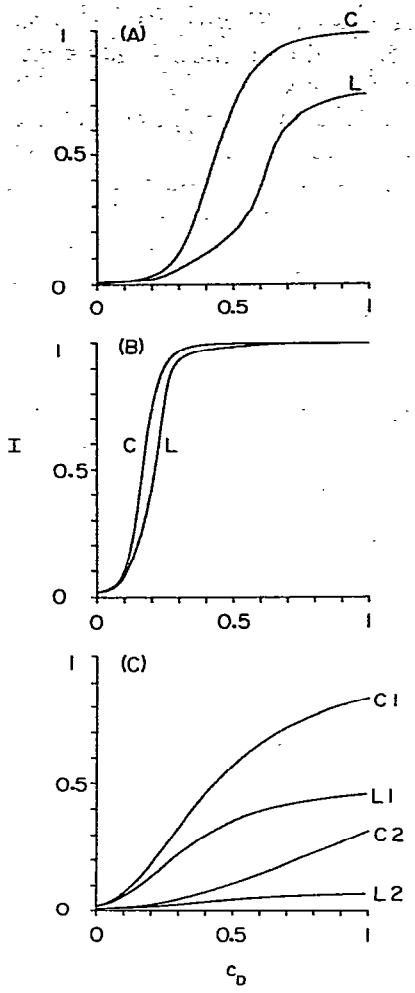

Fig. 3. Comparison of $I(c_D, c_T)$ from eq. (13) (L) to the predictions of the continuum theory of ref. [13] (C) for a square lattice of spacing a. (A) $c_T = 10^{-3}$; $w(r) = v(r) = k_D(R/r)^{14}$; $a/R = 0.6$; $q_D/q_T = 1$. (B) $c_T = 10^{-3}$, $w(r) = v(r) = k_D(R/r)^{14}$; $a/R = 0.4$; $q_D/q_T = 1$. (C) Curves C1 and L1 have the same parameters as (B) but with $w(r) = v(r) = k_D(R/r)^6$. Curves C2 and L2 have the same parameters as (A) but with $w(r) = v(r) = k_D(R/r)^6$. The continuum and lattice theories agree only for very low c_D and small a/R.

considerably from the two-dimensional case.

Most of the theories that have been developed for excitation or charge carrier transfer and trapping have been based on a continuum model [8–13], in which the particles are taken to be randomly distributed throughout some volume. Such theories are applicable to random solutions [18], but it is not clear to what extent they may be applied to substitutionally disordered crystals. Fig. 3 shows a comparison between the continuum trapping theory of ref. [13] and the lattice theory of the present work. Curve L in fig. 3A shows $I(c_D, c_T)$ for a square lattice, $c_T = 10^{-3}$, $w(r) = v(r) = k_D(R/r)^{14}$, $a/R = 0.6$, and curve L in fig. 3B shows $I(c_D, c_T)$ for the same system with $a/R = 0.4$. The curve labeled C in each figure is a calculation from the continuum theory of ref. [13] for a continuum with the same number densities of donors and traps and the same $w(r)$ and $v(r)$. The two theories agree at small values of c_D, and this agreement improves as the interaction length R becomes large relative to the lattice spacing. Fig. 3C shows the same calculations as 3A and 3B with transfer rates $w(r) = v(r) = k_D(R/r)^6$. (Note that for a given value of a/R, $w(a)$ will be much larger for the transfer rate of figs. 3A and 3B than for the transfer rate of fig. 3C.) The discrepancies between the lattice and continuum results can be large even for this longer-ranged transfer rate. These figures illustrate that the application of a continuum theory to experiments on mixed crystals may be inappropriate unless the interaction length is very large

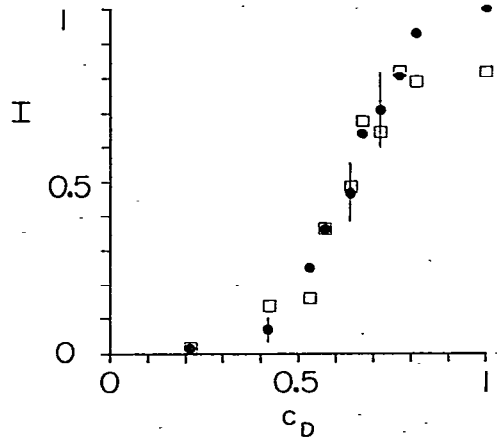

Fig. 4. The filled circles are measurements on singlet excitation transport in mixed naphthalene crystals at 4.2 K by Gentry and Kopelman [5]. The squares are calculated from eq. (13) for a square lattice and with the c_T values given by Gentry and Kopelman. $a/R = 0.60$, $q_D/q_T = 0.5$ and $w(r) = v(r) = k_D(R/r)^{14}$. The calculated points do not lie on a smooth curve because of the variation in c_T, which ranges from 3×10^{-4} to 1×10^{-3}.

relative to lattice parameters.

Singlet and triplet energy transport and trapping in an effectively two-dimensional system (perdeuteronaphthalene/naphthalene/betamethylnaphthalene mixed crystals) has been extensively studied by Kopelman and co-workers [4,5]. In our designation, naphthalene is the donor and betamethylnaphthalene is the trap. Measurements on singlet excitation transport on this system by Gentry and Kopelman [5] are depicted in fig. 4 (circles). c_T could not be kept exactly constant for these measurements, but varies from 3×10^{-4} to 1×10^{-3}. The squares in fig. 4 are the result of a two-body calculation of $I(c_D, c_T)$ for a square lattice with $q_D/q_T = 0.5$ (the value given by Gentry and Kopelman), $w(r) = v(r) = k_D(R/r)^{14}$, and $a/R = 0.6$. We have chosen an orientationally averaged octupole–octupole transfer rate because the transition dipole of naphthalene is known to be small and cannot account for the pure naphthalene crystal exciton band structure [19]. The octupole–octupole term is the next symmetry allowed term in a multipolar expansion of the intermolecular interaction [19]. We have assumed that transport is two dimensional, but it is unclear the extent to which this is true [4,5]. As discussed above, a small amount of transport between planes can have a large effect on this observable. The calculated points do not lie on a smooth curve as in figs. 1–3 because of the variation in trap concentration. The error bars on the data increase with increasing $I(c_D, c_T)$ because of difficulties in extracting the naphthalene fluorescence from the betamethylnaphthalene phonon sideband, which overlaps it [5]. The error bars on the three points at highest concentration are larger than the error bar on the point at $c_D = 0.72$ [20]. Within the experimental uncertainty, the calculated results and the data are in good agreement.

The agreement between the calculation and the data should not be interpreted as a proof that an incoherent hopping model is a valid description of energy transfer in naphthalene at 4.2 K. It is conceivable that such a model might apply for low donor concentration (strong spatial disorder) but that transfer is partially coherent at high donor concentration. The fact that a master equation approach may be least applicable at high c_D for low-temperature experiments may account for the discrepancy between data and calculation for the two points with highest c_D in fig. 4. The resolution of questions concerning the nature of energy transfer in mixed molecular crystals at low temperature must await theories that take into account incoherent phonon-assisted hopping among molecules with different site energies, and the possibility of partially coherent transfer. The results presented in this work will be applicable without ambiguity to energy and charge carrier transfer in mixed crystals at higher temperatures where an incoherent hopping model is known to be valid.

Acknowledgement

This work was supported by the National Science Foundation through grants CHE81-07165 (HCA) and DMR79-20380 (MDF and RFL). RFL thanks the National Science Foundation for a Predoctoral Fellowship. MDF acknowledges the Simon Guggenheim Memorial Foundation for Fellowship support that contributed to this research.

Appendix A. Diagrammatic expansion of the Green function

The expansion of $\hat{G}^s(\epsilon)$, $\hat{G}^m(k, \epsilon)$ and $G^T(k, \epsilon)$ (the Fourier–Laplace transforms of eqs. (4) in powers of the transfer matrix $\mathbf{Q}$ can be carried out with the procedure described in detail in section 3 of I, and will not be discussed further here. The representation of the terms in these expansions by diagrams is completely analogous to the corresponding procedure in section 3 of I. The ith donor is represented by a circle labeled i, and jth trap is represented by a square labeled j. A factor $w_{ij}(v_{ij})$ is represented by a solid arrow from circle j to circle (square) i. Each solid arrow begins in a solid dot denoted a vertex, which has a value ϵ^{-1}, and ends in a point that may or may not be a vertex depending upon whether it is the beginning of another solid arrow. A factor $-w_{ij}(-v_{ij})$ is represented by a solid arrow from circle j to circle (square) i

followed by a dashed arrow returning to circle j. Thus a dashed arrow can only begin at the end of a solid arrow and must return to the circle in which the solid arrow begins. The last arrow in the diagram, solid or dashed, ends in a vertex. A factor $-\delta_{r_i,r_j}$ is represented by a wavy line connecting the circles or squares labeled i and j. $\hat{G}^{\mathrm{m}}(k,\epsilon)$ diagrams are characterized by a continuous path of solid and dashed arrows beginning on an initial circle labeled 1 and ending on a final circle labeled 2. Circles 1 and 2 are denoted root circles and other circles (squares) visited on the path are denoted field circles (squares). Since transfer out of a trap is forbidden, a trap square in a $\hat{G}^{\mathrm{m}}(k,\epsilon)$ diagram may not contain a vertex. $\hat{G}^{\mathrm{T}}(k,\epsilon)$ diagrams are characterized by a continuous path of solid and dashed arrows beginning on an initial circle labeled 1 and ending on a final square labeled $N_{\mathrm{D}}+1$. Circle 1 and square $N_{\mathrm{D}}+1$ are denoted roots and other circles (squares) are denoted field circles (squares). The last arrow in each $\hat{G}^{\mathrm{T}}(k,\epsilon)$ diagram ends on a vertex in square $N_{\mathrm{D}}+1$. This must be the only trap vertex in the diagram. $\hat{G}^{\mathrm{s}}(\epsilon)$ diagrams have a single root circle labeled 1, one or more field circles (squares), and a continuous path of solid and dashed arrows that begins and ends on the root. As in $\hat{G}^{\mathrm{m}}(k,\epsilon)$, there may be no trap vertices.

We will base our discussion of these diagrams on the diagrammatic expansion of the Green function for the continuum transport and trapping problem presented in ref. [12]. We denote by g^{s}, g^{m} and g^{T} the diagrammatic expansions of $\hat{G}^{\mathrm{s}}(\epsilon)$, $\hat{G}^{\mathrm{m}}(k,\epsilon)$and $\hat{G}^{\mathrm{T}}(k,\epsilon)$ for the continuum problem given in eq. (18), eq. (20) and eq. (22) of ref. [12]. It should be emphasized that the symbols g^{s}, g^{m} and g^{T} represent sets of diagrams and *not* the values assigned to these diagrams in ref. [12]. In analogy with eqs. (III.10) and (III.11) of I, we can write

$$\hat{G}^{\mathrm{s}}(\epsilon) = \epsilon^{-1} + g^{\mathrm{s}} + \text{the infinite series of diagrams constructed by adding to } g^{\mathrm{s}} \text{ diagrams at most one wavy line between each pair of donor circles, each pair of trap squares, and each donor–trap pair. Two circles or two squares or a circle and a square may be connected by a wavy line only if there does not exist a solid arrow that begins in one and ends in the other.} \tag{A1}$$

$$\hat{G}^{\mathrm{m}}(k,\epsilon) = g^{\mathrm{m}} + \text{the sum of all diagrams derived from } g^{\mathrm{m}} \text{ by introducing wavy lines in the manner described in eq. (A1).} \tag{A2}$$

$$\hat{G}^{\mathrm{T}}(k,\epsilon) = g^{\mathrm{T}} + \text{the sum of all diagrams derived from } g^{\mathrm{T}} \text{ by introducing wavy lines in the manner described in eq. (A1).} \tag{A3}$$

In the thermodynamic limit, these diagrams are evaluated as follows. The field circles (squares) are assigned dummy labels. A solid arrow from circle j to circle i is assigned a factor w_{ij}. A solid arrow from circle j to square i is assigned a factor v_{ij}. Each vertex is assigned a factor ϵ^{-1}. Each wavy line is assigned a factor $-\delta_{r_i,r_j}$. Each dashed arrow is assigned a factor -1. This product is multiplied by $\exp(\mathrm{i}\boldsymbol{k}\cdot\boldsymbol{r}_{21})$ for a $\hat{G}^{\mathrm{m}}(k,\epsilon)$ diagram or by $\exp(\mathrm{i}\boldsymbol{k}\cdot\boldsymbol{r}_{N_{\mathrm{D}}+1,1})$ for a $\hat{G}^{\mathrm{T}}(k,\epsilon)$ diagram. The positions of the second root (for $\hat{G}^{\mathrm{m}}(k,\epsilon)$ and $\hat{G}^{\mathrm{T}}(k,\epsilon)$) and of any field circles (squares) are summed over all lattice sites. These sums are unrestricted, since the δ_{r_i,r_j} factors correct for configurations in which more than one donor or trap is allowed to occupy the same site. The result is then multiplied by $c_{\mathrm{D}}^{m-1}c_{\mathrm{T}}^{n}$, where m is the number of donor circles and n is the number of trap squares.

The diagrammatic expansions of $\hat{G}^{\mathrm{m}}(k,\epsilon)$ and $\hat{G}^{\mathrm{T}}(k,\epsilon)$ can be simplified by using a topological reduction procedure as described in section 4 of I to eliminate loops. A loop is a part of a diagram that becomes disconnected from both root circles by the removal of a single circle and of a pair of vertices within that circle. A more detailed definition is given in footnote 13 of I. We can exactly rewrite the diagrammatic expansions of $\hat{G}^{\mathrm{m}}(k,\epsilon)$ and $\hat{G}^{\mathrm{T}}(k,\epsilon)$ as new series without loops in which the vertices now carry a value $\hat{G}^{\mathrm{s}}(\epsilon)$ rather than ϵ^{-1}. Eqs. (A2) and (A3) can be replaced by

$$\hat{G}^{\mathrm{m}}(k,\epsilon) = \text{the sum of all diagrams in eq. (A2) without loops. These diagrams are evaluated by the same procedure as those in eq. (A2) except that all vertices are assigned the value } \hat{G}^{\mathrm{s}}(\epsilon) \text{ instead of } \epsilon^{-1}. \tag{A4}$$

$\hat{G}^{T}(k, \epsilon)$ = the sum of all diagrams in eq. (A3) without loops. These diagrams are evaluated by the same procedure as those in eq. (A3) except that all vertices *but the trap vertex* are assigned the value $\hat{G}^{s}(\epsilon)$. The trap vertex retains the value ϵ^{-1}. (A5)

An important topological feature in the diagrams of eqs. (A4) and (A5) is the node. A node is a vertex in a field circle with the property that removal of the field circle and of that one vertex within it leaves the two roots disconnected. A more detailed definition is given in footnote 15 of I. All of the diagrams in eqs. (A4) and (A5) can be generated from the subset of diagrams in each equation that have no nodes. We define $\Sigma_{D}(k, \hat{G}^{s}(\epsilon))$ and $\Sigma_{T}(k, \hat{G}^{s}(\epsilon))$ by

$$\Sigma_{D}(k, \hat{G}^{s}(\epsilon)) = 1/c_{D}\left[\hat{G}^{s}(\epsilon)\right]^{2} \text{ [sum of all diagrams in eq. (A4) without nodes]}, \tag{A6}$$

$$\Sigma_{T}(k, \hat{G}^{s}(\epsilon)) = \epsilon/c_{T}\hat{G}^{s}(\epsilon) \text{ [sum of all diagrams in eq. (A5) without nodes]}. \tag{A7}$$

Both $\Sigma_{D}(k, \hat{G}^{s}(\epsilon))$ and $\Sigma_{T}(k, \hat{G}^{s}(\epsilon))$ depend on ϵ only through $\hat{G}^{s}(\epsilon)$. Expressions relating $\hat{G}^{m}(k, \epsilon)$ and $\hat{G}^{T}(k, \epsilon)$ to $\Sigma_{D}(k, \hat{G}^{s}(\epsilon))$ and $\Sigma_{T}(k, \hat{G}^{s}(\epsilon))$ are given in eqs. (7).

Appendix B. Evaluation of $\bar{\Sigma}_{D}^{(2)}$ and $\bar{\Sigma}_{T}^{(2)}$

In appendices B and C we discuss the evaluation of those contributions to the two-body approximations of Σ_{D} and Σ_{T} that are of order c_{T}. In summing these diagrams we will use many of the results and techniques introduced in appendices A, B, and C of I.

We begin by renormalizing the $\bar{\Sigma}_{D}^{(2)}$ and $\bar{\Sigma}_{T}^{(2)}$ diagrams using the topological theorem presented in appendix C of I. Although traps are represented by squares and donors by circles in our diagrammatic notation, we will use the term "circle" for convenience in the following discussion to mean either a donor or a trap. In examining a $\bar{\Sigma}_{D}^{(2)}$ or $\bar{\Sigma}_{T}^{(2)}$ diagram it is useful to group the circles into sets such that all circles in a given set are connected to each other by wavy lines and circles in one set are not connected to circles in another set by wavy lines. In appendix A of I, we rewrote the $\Sigma_{D}^{(2)}$ series in the absence of traps as a new series with restrictions on allowed wavy line connections among the circles in a set. We will follow an analogous procedure here with the more complicated trapping diagrams.

A set of circles in a $\bar{\Sigma}_{D}^{(2)}$ or $\bar{\Sigma}_{T}^{(2)}$ diagram either contains no traps or one trap. If it contains no traps, we treat it as we did in appendix A of I. If it contains a trap, it must fall into one of two categories: (i) the set contains zero or one donor root circles ($\bar{\Sigma}_{D}^{(2)}$ or $\bar{\Sigma}_{T}^{(2)}$), (ii) the set contains two donor root circles ($\bar{\Sigma}_{D}^{(2)}$ only). A consequence of the topological theorem of appendix C in I is that we need only retain diagrams in which each set of circles is connected by some arbitrarily specified singly connected path of wavy lines. (The remaining diagrams have a total value of zero for any choice of the singly connected path.) When the diagram is evaluated, such a path linking a set of n circles contributes a factor $(n-1)!$. This singly connected path may be specified for a set of n circles by assigning numerical labels 1 through n to the circles according to some rule. The only allowable wavy line path is one constructed by linking circle i to circle $i+1$ with a wavy line for $i = 1, 2, \cdots n-1$. It is most convenient to adopt two different procedures for specifying the allowed wavy line connections among a set of n circles containing a trap, depending on whether the set belongs to category (i) or (ii).

Consider the $\bar{\Sigma}_{T}^{(2)}$ diagrams A through D in fig. 5 *. They differ from each other in the placement of wavy lines within a set of circles. Such diagrams are denoted topologically similar [1]. Since a wavy line carries a value $-\delta_{r_i, r_k}$, two topologically similar diagrams have values that differ only by a factor of ± 1.

* Since $\bar{\Sigma}_{T}^{(2)}$ and $\bar{\Sigma}_{D}^{(2)}$ diagrams contain at most one trap, the dummy label $N_{D}+1$ will be omitted from the trap in figs. 5–9.

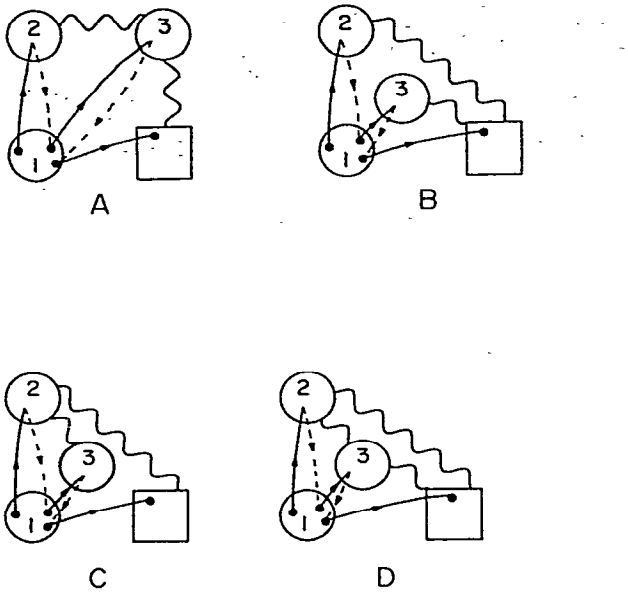

Fig. 5. Four topologically similar $\bar{\Sigma}_T^{(2)}$ diagrams. See text for discussion.

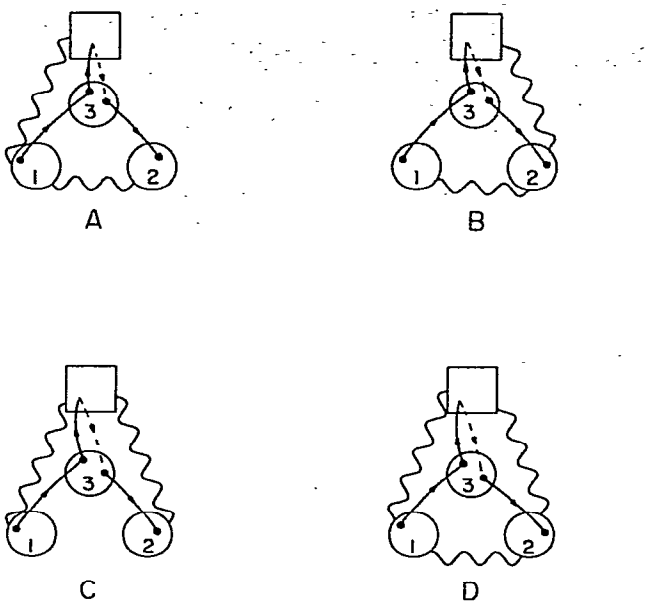

Fig. 6. Four topologically similar $\bar{\Sigma}_D^{(2)}$ diagrams in which two donor root circles and a trap are linked together by wavy lines. See text for discussion.

There is thus considerable cancellation in a sum of a group of topologically similar diagrams. The set of circles containing the trap in A–D falls into category (i). In this case we choose the singly connected path of wavy lines to be the one constructed by drawing a wavy line from the trap to the first donor in the set to be visited by solid arrows, from that donor to the next donor to be visited by solid arrows, and so on. When the diagram is evaluated, that path contributes a factor $(n-1)!$ where n is the number of circles in the set. This means that we will represent the sum of A–D with the symbol of diagram C, whose value now has an additional factor of 2!. This procedure can be verified for this example by noting that diagrams A, B and C have the same value and diagram D has a value that differs by a factor of -1.

Now consider $\bar{\Sigma}_D^{(2)}$ diagrams A–D in fig. 6. The set of circles containing the trap in diagrams A–D falls into category (ii). In this case we choose to represent the sum of a group of topologically similar diagrams by a diagram in which the wavy line path is constructed by connecting the trap to the first root, the first root to the second root, the second root to the first donor field circle to be visited by solid arrows, that circle to the next donor field circle to be visited by solid arrows, and so on. We represent the sum of diagrams A–D with the symbol of diagram A, whose value now contains a factor 2!. This result can be verified by noting that diagrams A, B and C have identical values and that the value of diagram D differs by a factor of -1.

We have simplified the diagrammatic expansion of $\bar{\Sigma}_D^{(2)}$ and $\bar{\Sigma}_T^{(2)}$ by grouping together diagrams whose values differ only by factors of -1. We now group together diagrams whose values differ only by a factor made up of an integer and a power of $-c_D$. We define the notion of the reduced diagram, introduced in appendix A of I. A reduced diagram is derived from a $\bar{\Sigma}_T^{(2)}$ or $\bar{\Sigma}_D^{(2)}$ diagram by collapsing all wavy lines except wavy lines connecting a donor to a trap or a donor root circle to a second donor root circle. A wavy line connecting circles A and B is collapsed [1] by moving all ends of solid arrows in circle A to circle B and then removing circle A and the wavy line. This reduced diagram is always itself a member of $\bar{\Sigma}_D^{(2)}$ or $\bar{\Sigma}_T^{(2)}$. A diagram with no wavy lines or whose only wavy lines connect two donor roots or a donor and a trap is its own reduced diagram. Two diagrams with the same reduced diagram have values that differ only by a

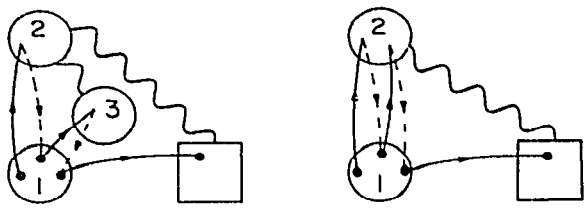

Fig. 7. Diagrams A and B have B as a reduced diagram. See text for discussion.

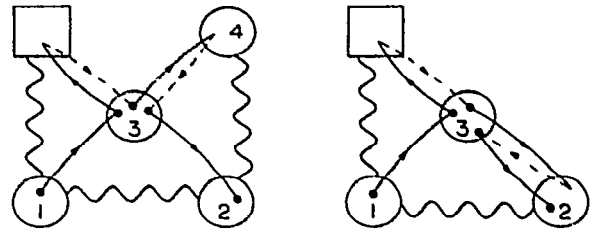

Fig. 8. Diagrams A and B have B as a reduced diagram. See text for discussion.

factor made up of an integer and a power of $-c_D$. We will represent the set of all diagrams with the same reduced diagram by that reduced diagram in the renormalized $\bar{\Sigma}_T^{(2)}$ and $\bar{\Sigma}_D^{(2)}$ series. The value of the reduced diagram now contains a factor of a polynomial in $-c_D$. In fig. 7, diagrams A and B both have diagram B as a reduced diagram. If diagram B has value V, then diagram A has value $-2c_DV$. We represent their sum by the symbol of diagram B, whose value now includes a factor of $1-2c_D$. In fig. 8, diagrams A and B both have B as a reduced diagram. The value of diagram A differs from the value of diagram B by a factor of $-3c_D$. We represent their sum by diagram B whose value now includes a factor of $1-3c_D$. The value of B also includes a factor of 2! for the wavy line path and it will be useful later to combine these factors into a polynomial $2-6c_D$.

Each circle in a renormalized $\bar{\Sigma}_D^{(2)}$ or $\bar{\Sigma}_T^{(2)}$ diagram has an associated polynomial, because the collapsing of wavy lines in one set of circles is carried out independently of the collapsing of wavy lines in another set. We modify the definition of the moveable part in I to apply to the trapping diagrams. For root circle 1, a moveable part is any end of a solid arrow to visit the circle, unless root 1 is connected by wavy lines to root 2 and to the trap. In this case, root 1 has no moveable parts. For any other donor circle, a moveable part is any end of a solid arrow in the circle except for the end of the last solid arrow to visit the circle. We use "end" here in the sense of I. Each arrow has one beginning and one end, with the arrow head pointing from the beginning to the end. In I for the lattice transport problem, we showed that a circle with n moveable parts in the renormalized series has an associated nth degree polynomial $Q_n(c_D)$, whose form is derived in appendix A of that work. In a renormalized $\bar{\Sigma}_D^{(2)}$ or $\bar{\Sigma}_T^{(2)}$ diagram in the present problem, a donor circle with n moveable parts also has an associated nth degree polynomial in $-c_D$, but this polynomial may be of three different forms.

A donor circle with no wavy line connection and with n moveable parts carries a factor $Q_n(c_D)$. Two donor roots, connected to each other but not to a trap by a wavy line, each carry factors of $Q_n(c_D)$. A donor circle with n moveable parts connected only to a trap by a wavy line carries a factor $R_n(c_D)=\mathrm{d}[c_DQ_nc_D)]/\mathrm{d}c_D$. This result can be verified for the example of fig. 7. The sum of A and B in the original $\bar{\Sigma}_T^{(2)}$ series is represented by diagram B in the renormalized $\bar{\Sigma}_T^{(2)}$ series. The renormalized diagram now has a factor of $1-2c_D$ associated with circle 2. Since $Q_1(c_D)=1-c_D$, $R_1(c_D)=1-2c_D$. The last possibility is illustrated by diagram B in fig. 8. A wavy line path connects a trap to one donor root and that circle to the other donor root. For such diagrams, the first donor has no moveable parts, as stated above. If the second donor has n moveable parts, it has an associated factor of $S_n(c_D)=\mathrm{d}^2[c_D^2Q_n(c_D)]/\mathrm{d}c_D^2$. This result can be verified for the example of diagram B in fig. 8, for which circle 2 was demonstrated to have an associated

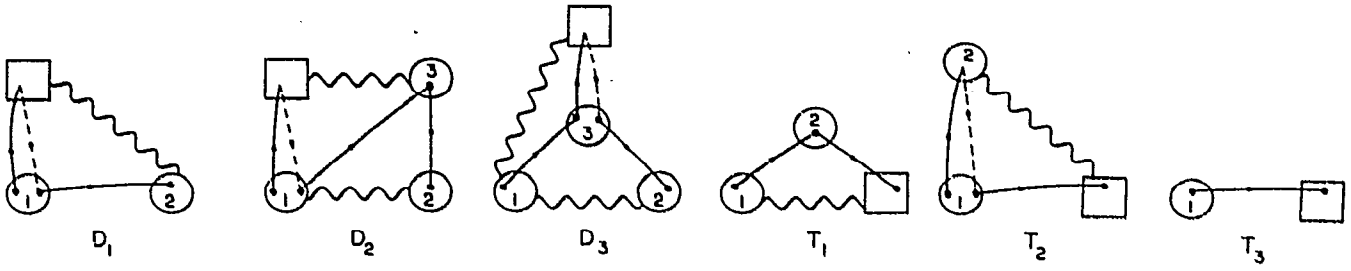

Fig. 9. Representative examples of the three groups of $\bar{\Sigma}_D^{(2)}$ diagrams (D_1, D_2, D_3) that compose the $\bar{\Sigma}_D^{(2)}$ series and of the three groups of $\bar{\Sigma}_T^{(2)}$ diagrams (T_1, T_2, T_3) that compose the $\bar{\Sigma}_T^{(2)}$ series.

polynomial of $2-6c_D$. Since $Q_1(c_D)=1-c_D$, $S_1(c_D)=2-6c_D$.

We can now present the diagrams in the renormalized $\bar{\Sigma}_D^{(2)}$ and $\bar{\Sigma}_T^{(2)}$ series that are of order c_T. It is most convenient to divide the diagrams in the following groups and then to sum each group separately. Representative members of each of the groups are shown in fig. 9. D_1: These $\bar{\Sigma}_D^{(2)}$ diagrams have two donor root circles, and one trap, with a wavy line connecting one of the roots to the trap. D_2: These $\bar{\Sigma}_D^{(2)}$ diagrams have two donor root circles, a trap and a donor field circle. The two roots are connected by a wavy line as are the trap and circle 3. D_3: These $\bar{\Sigma}_D^{(2)}$ diagrams have two donor roots, a trap and a donor field circle. The trap is connected to the first root by a wavy line, and the first root is connected to the second root by a wavy line. T_1: These $\bar{\Sigma}_T^{(2)}$ diagrams have one donor field circle and a wavy line between the roots. T_2: These $\bar{\Sigma}_T^{(2)}$ diagrams have one donor field circle and a wavy line between the trap and the field circle. T_3: These $\bar{\Sigma}_T^{(2)}$ diagrams have no field circles and hence no wavy lines.

These sums of diagrams can be evaluated using the techniques of appendix B of I. As an example we carry out the summation of the D_2 series in detail in appendix C of this work. The final results are presented below.

$$D_1 = -2c_T\sum_r e^{ik\cdot r}w(r)\left[\int_0^\infty d\alpha\, e^{-\alpha}\frac{e^{-z\alpha}}{1-c_D+c_D e^{-z\alpha}} \times\left(\frac{\theta e^{-z\alpha\theta}}{(1-c_D+c_D e^{-z\alpha\theta})^2}-\frac{e^{-z\alpha}}{(1-c_D+c_D e^{-z\alpha})^2}\right)\right], \tag{B1}$$

$$D_2 = -c_T\sum_r w(r)\int_0^\infty d\alpha\, e^{-\alpha}\left((1/c_D)\ln(1-c_D+c_D e^{-z\alpha})+\frac{(1-c_D)(1-e^{-z\alpha})}{1-c_D+c_D e^{-z\alpha}}\right) \times\left(\frac{\theta^2 e^{-z\alpha\theta}}{(1-c_D+c_D e^{-z\alpha\theta})^2}-\frac{e^{-z\alpha}}{(1-c_D+c_D e^{-z\alpha})^2}\right), \tag{B2}$$

$$D_3 = -2c_T\sum_r w(r)\int_0^\infty d\alpha\, e^{-\alpha}\frac{e^{-z\alpha}}{1-c_D+c_D e^{-z\alpha}} \times\left(\frac{e^{-z\alpha}+(1-c_D)/2c_D}{(1-c_D+c_D e^{-z\alpha})^2}-\frac{e^{-z\alpha\theta}+(1-c_D)/2c_D}{(1-c_D+c_D e^{-z\alpha\theta})^2}\right), \tag{B3}$$

$$T_1 = -c_D\sum_r v(r)z\int_0^\infty d\alpha\, e^{-\alpha}\left(\frac{e^{-z\alpha}}{1-c_D+c_D e^{-z\alpha}}\right)\left(\frac{\theta e^{-z\alpha\theta}}{(1-c_D+c_D e^{-z\alpha\theta})^2}\right), \tag{B4}$$

$$T_2 = c_D \sum_r e^{ik\cdot r} v(r) z \int_0^\infty e^{-\alpha} d\alpha \left(\frac{e^{-z\alpha}}{1 - c_D + c_D e^{-z\alpha}} \right) \left(\frac{\theta^2 e^{-z\alpha\theta}}{(1 - c_D + c_D e^{-z\alpha\theta})^2} \right), \tag{B5}$$

$$T_3 = \sum_r e^{ik\cdot r} v(r) \theta. \tag{B6}$$

z and θ are defined in section 3.

Appendix C. Evaluation of the D_2 series of appendix B

In appendix B, D_2 is defined to be the sum of all diagrams in $\bar{\Sigma}_D^{(2)}$ with two donor root circles (labeled 1 and 2) connected by a wavy line and a trap field circle and a donor field circle (labeled 3) that are also connected by a wavy line. An example of a D_2 diagram is shown in fig. 9. This series of diagrams is easiest to sum by first examining a fictitious diagrammatic series F_2. The diagrams in F_2 are identical to the diagrams in D_2. The value of an F_2 diagram differs from the value of the corresponding D_2 diagram in that instead of associating a polynomial in $-c_D$ with each donor circle, we assign a moveable part on root 1 a value of m_1, a moveable part on root 2 a value m_2 and a moveable part on circle 3 a value m_3. We define renormalized transfer rates from circle 1 to circle 3 and from circle 2 to circle 3 by

$$w_{13}(r) = w_{23}(r) \equiv w'(r) \equiv w(r)/[1 + \hat{G}^s(\epsilon) v(r)]. \tag{C1}$$

These renormalized transfer rates include all possible excursions to the trap from a given vertex on circle 1 or circle 3. Since there are no solid arrow connections between circle 3 and the trap, transfer rates w_{31} and w_{32} are not renormalized in this way:

$$w_{31}(r) = w_{32}(r) \equiv w(r). \tag{C2}$$

By utilizing the renormalization in eq. (C1), we include a set of diagrams that are of order $[v(r)]^0$, which do not belong in D_2. We will sum series $\tilde{D}_2$ and $\tilde{F}_2$ that include this spurious contribution and then subtract it off as a final step to recover D_2. Since the presence of the trap has been entirely accounted for by the renormalization of eq. (C1), the problem of summing the $\tilde{F}_2$ series is very similar to the problem of summing the $E_s^{(2)}$ series in appendix A of I, except that the transfer rates are now asymmetric: $w_{13} \neq w_{31}$. We define generalized transfer rates

$$T_{13} = \frac{w'(r)}{1 + m_3 w'(r) \hat{G}^s(\epsilon)}, \qquad T_{32} = \frac{w(r)}{1 + m_3 w'(r) \hat{G}^s(\epsilon)}, \tag{C3}$$

and generalized return rates

$$R_{31} = \frac{-w(r) \hat{G}^s(\epsilon) m_1}{1 + m_3 w'(r) \hat{G}^s(\epsilon)}, \qquad R_{32} = \frac{-w(r) \hat{G}^s(\epsilon) m_2}{1 + m_3 w'(r) \hat{G}^s(\epsilon)}. \tag{C4}$$

The series $\tilde{F}_2$ can be written as

$$\begin{aligned} \tilde{F}_2 &= c_D c_T \hat{G}^s(\epsilon) \sum_r T_{13} T_{32} \theta \sum_{i=0}^{\infty} (R_{31} + R_{32})^i \\ &= c_D c_T \hat{G}^s(\epsilon) \sum_r [w'(r)]^2 \left(\frac{1}{1 + \theta z m_3} \right) \left(\frac{1}{1 + z(m_1 + m_2 + \theta m_3)} \right). \end{aligned} \tag{C5}$$

z and θ are defined in section 3. Expanding eq. (C5) in powers of z yields

$$\tilde{F}_2 = c_D c_T \hat{G}^s(\epsilon) \sum_r [w'(r)]^2 \sum_{i=0}^{\infty} (-z)^i \sum_{j=1}^{i+1} \binom{i+1}{j} (\theta m_3)^{i+1-j} \sum_{l=0}^{j-1} \binom{j-1}{l} m_1^l m_2^{j-1-l}. \tag{C6}$$

An $\tilde{F}_2$ diagram with a factor $m_3^{i+1-j}\, m_1^l m_2^{j-1-l}$ corresponds to a $\tilde{D}_2$ diagram with a factor $R_{i+1-j}(c_D) Q_l(c_D) Q_{j-1-l}(c_D)$. We can therefore write

$$\tilde{D}_2 = c_D c_T \hat{G}^s(\epsilon) \sum_r [w'(r)]^2 \sum_{i=0}^{\infty} (-z)^i \sum_{j=1}^{i+1} \binom{i+1}{j} \theta^{i+1-j} R_{i+1-j}(c_D) \times \sum_{l=0}^{j-1} \binom{j-1}{l} Q_l(c_D) Q_{j-1-l}(c_D). \tag{C7}$$

From eq. (B7) of I, we have

$$Q_n(c_D) = \frac{d^n}{dy^n} \left(\frac{e^y}{1 - c_D + c_D e^y} \right) \Bigg|_{y=0} \tag{C8}$$

and therefore

$$R_n(c_D) = \frac{d^n}{dy^n} \left(\frac{e^y}{(1 - c_D + c_D e^y)^2} \right) \Bigg|_{y=0}. \tag{C9}$$

From eq. (C8) and Leibnitz' rule,

$$\sum_{l=0}^{j-1} \binom{j-1}{l} Q_l(c_D) Q_{j-1-l}(c_D) = \frac{d^{j-1}}{dy^{j-1}} \left(\frac{e^y}{1 - c_D + c_D e^y} \right)^2 \Bigg|_{y=0}. \tag{C10}$$

Substituting eqs. (C9) and (C10) into the sum over i in eq. (C7) gives

$$\sum_{i=0}^{\infty} (-z)^i \sum_{j=1}^{i+1} \binom{i+1}{j} \theta^{i+1-j} \frac{d^{i+1-j}}{dy^{i+1-j}} \left(\frac{e^y}{(1 - c_D + c_D e^y)^2} \right) \Bigg|_{y=0} \frac{d^{j-1}}{dy^{j-1}} \left(\frac{e^y}{1 - c_D + c_D e^y} \right)^2 \Bigg|_{y=0}$$

$$= \sum_{i=0}^{\infty} (-z)^i \sum_{j=1}^{i+1} \binom{i+1}{j} \frac{d^{i+1-j}}{dy^{i+1-j}} \left(\frac{e^{\theta y}}{(1 - c_D + c_D e^{\theta y})^2} \right) \Bigg|_{y=0}$$

$$\times \frac{d^j}{dy^j} \left(-\frac{1}{c_D} \frac{e^y}{1 - c_D + c_D e^y} + \frac{1}{c_D^2} \ln(1 - c_D + c_D e^y) \right) \Bigg|_{y=0}. \tag{C11}$$

Applying Leibnitz' rule to the right-hand side of eq. (C11) gives

$$\sum_{i=0}^{\infty} (-z)^i \frac{d^{i+1}}{dy^{i+1}} \left(\frac{e^{\theta y}}{(1 - c_D + c_D e^{\theta y})^2} \right) \left(-\frac{1}{c_D} \frac{e^y}{1 - c_D + c_D e^y} + \frac{1}{c_D^2} \ln(1 - c_D + c_D e^y) + \frac{1}{c_D} \right) \Bigg|_{y=0}. \tag{C12}$$

We can perform the summation over i using the identity

$$\sum_{k=0}^{\infty} (x)^k d^k L(y)/dy^k|_{y=0} = \int_0^{\infty} d\alpha\, e^{-\alpha} L(x\alpha), \tag{C13}$$

where $L(x)$ is analytic at $x = 0$. The final result is

$$\tilde{D}_2 = -c_T \sum_r \theta^2 w(r) \int_0^\infty d\alpha\, e^{-\alpha} \frac{e^{-\alpha\theta z}}{\left(1 - c_D + c_D e^{-\alpha\theta z}\right)^2} \times \left((1/c_D) \ln(1 - c_D + c_D e^{-\alpha z}) + \frac{(1 - c_D)(1 - e^{-\alpha z})}{1 - c_D + c_D e^{-\alpha z}} \right). \tag{C14}$$

As discussed above, to obtain the D_2 sum from $\tilde{D}_2$, we must subtract off the spurious contribution of order $[v(r)]^0$:

$$D_2 = -c_T \sum_r w(r) \int_0^\infty d\alpha\, e^{-\alpha} \left(\frac{\theta^2 e^{-\alpha\theta z}}{\left(1 - c_D + c_D e^{-\alpha\theta z}\right)^2} - \frac{e^{-\alpha z}}{\left(1 - c_D + c_D e^{-\alpha z}\right)^2} \right) \times \left((1/c_D) \ln(1 - c_D + c_D e^{-\alpha z}) + \frac{(1 - c_D)(1 - e^{-\alpha z})}{1 - c_D + c_D e^{-\alpha z}} \right). \tag{C15}$$

References

[1] R.F. Loring, H.C. Andersen and M.D. Fayer, J. Chem. Phys. (1984), to be published.

[2] D.D. Smith, R.D. Mead and A.H. Zewail, Chem. Phys. Letters 50 (1977) 358.

[3] S.D. Colson, S.M. George, T. Keyes and V. Vaida, J. Chem. Phys. 67 (1977) 4941.

[4] R. Kopelman, in: Topics in applied physics, Vol. 49, eds. W.M. Yen and P.M. Seltzer (Springer, Berlin, 1981) p. 241.

[5] S.T. Gentry and R. Kopelman, J. Chem. Phys. 78 (1983) 373;
S.T. Gentry, Ph.D. Thesis, University of Michigan, Ann Arbor, Michigan (1983).

[6] D.D. Dlott, M.D. Fayer and R.D. Wieting, J. Chem. Phys. 69 (1978) 2752.

[7] G.F. Imbusch, Phys. Rev. 153 (1967) 326.

[8] D.L. Huber, Phys. Rev. B20 (1979) 2307.

[9] D.L. Huber, Phys. Rev. B20 (1979) 5333.

[10] A. Blumen and R. Silbey, J. Chem. Phys. 70 (1979) 3707.

[11] B. Movaghar and G.W. Sauer, J. Phys. C13 (1980) 4933.

[12] R.F. Loring, H.C. Andersen and M.D. Fayer, J. Chem. Phys. 76 (1982) 2015.

[13] R.F. Loring and M.D. Fayer, Chem. Phys. 70 (1982) 139.

[14] V. Sakun, Soviet Phys. Solid State 14 (1973) 1906.

[15] V.M. Kenkre and P.E. Parris, Phys. Rev. B27 (1983) 3221.

[16] C.R. Gochanour, H.C. Andersen and M.D. Fayer, J. Chem. Phys. 70 (1979) 4254.

[17] T. Keyes and S. Pratt, Chem. Phys. Letters 65 (1979) 100.

[18] R.J.D. Miller, M. Pierre and M.D. Fayer, J. Chem. Phys. 78 (1983) 5138.

[19] D.P. Craig and S.H. Walmsley, Excitons in molecular crystals (Benjamin, New York, 1968) p. 107.

[20] R. Kopelman, private communication.